Sustainable Production of Gluconic Acid and Glucuronic Acid via Microwave-Assisted Glucose Oxidation over Low-Cost Cu Biochar Catalyst

Supplementary Information

Qiaozhi Zhang [1, 2], Shuguang Xu[1, 2, 3], Yang Cao [1, 2], Roger Ruan [4], James H. Clark [5], Changwei Hu [3], Daniel C.W. Tsang [1, 2, *]

[1] Department of Civil and Environmental Engineering, The Hong Kong Polytechnic University, Hung Hom, Kowloon, Hong Kong, China.

[2] Research Institute for Future Food, The Hong Kong Polytechnic University, Hung Hom, Kowloon, Hong Kong, China.

[3] Key Laboratory of Green Chemistry and Technology, Ministry of Education, College of Chemistry, Sichuan University, Chengdu, Sichuan, 610064, China.

[4] Center for Biorefining and Department of Bioproducts and Biosystems Engineering, University of Minnesota, 1390 Eckles Ave., St. Paul, MN 55108, United States

[5] Green Chemistry Centre of Excellence, Department of Chemistry, University of York, York, YO10 5DD, UK

* Corresponding author: Prof. Daniel Tsang, dan.tsang@polyu.edu.hk

Table of Contents

S1. Chemicals

The $CuCl_2 \cdot 2H_2O$ (> 99%, AR, UNI-CHEM) was used as precursor of loaded Cu. The chemicals for reaction and characterizations mainly included the oxidant H_2O_2 (30 wt%, Honeywell), substrate glucose (AR, Aladdin), standard gluconic acid (GOA, 49-53 wt% in aqueous solution, Sigma-Aldrich), standard glucuronic acid (GUA, > 98%, Sigma-Aldrich), and standard 5-keto-gluconic acid potassium salt (> 98%, Sigma-Aldrich).

S2. Characterization Method

S2.1 Pre-treatment and detailed method

Before Inductively Coupled Plasma Optical Emission Spectroscopy (ICP-OES) measurement, 20 mg of biochar catalyst was burnt in muffle furnace at 700 °C for 30 min and the residue was then digested by 2 mL of concentrated HNO_3 until the liquid phase was completely evaporated. Afterward, the residual solid was dissolved and diluted with 5% HNO_3 to the calibration range of concentration and filtered through a mixed cellulose easter membrane (pore size 0.45 μm).

Hydrogen Temperature-programmed Reduction (H_2-TPR) was performed after a pre-treatment at 100 °C for 1 h with Ar purging flow rate of 30 mL/min.

Each sample was filtered by a mixed cellulose easter membrane (pore size 0.45 μm) before the HPLC measurement. The reason for using two detectors (*i.e.*, Refractive Index (RI) detector and Ultraviolet-visible (UV-Vis) detector) to quantify glucose and GOA concentration was that these two compounds could not be separated (*i.e.*, their retention time were the same). Despite this limitation, their concentrations could be quantified due to their different signal response: GOA could be detected by both UV-Vis detector and RI detector, while glucose could only be detected by RI detector and not be detected by UV-Vis detector at 210 nm. Therefore, their concentrations could be calculated by subtraction.

S2.2 Post-treatment of data

All experiments were conducted at least in duplicate, and the results were presented as mean value ± standard deviation. One-way analysis of variance (ANOVA) was utilized to determine the significance of differences ($p < 0.05$) of data sets by IBM SPSS Statistics 26. The significance levels were labelled in figures or listed in tables as lower-case letters.

For the Elemental Analysis, the weight ratio of O could not be directly measured, which was calculated by subtracting the weight summary of other detectable elements (*i.e.*, C, H, and N) and ash from the initial weight.

The XRD patterns were obtained with a low speed of 1°/min to improve the resolution of the patterns. The information of these patterns (*e.g.*, peak position, peak intensity, half the maximum intensity (FWHM), etc.) was determined by MDI JADE 6. Based on the XRD patterns, the mean size of the crystalline domains (τ) was calculated by Scherrer Equation (Eq. S1),

$$\tau = \frac{K\lambda}{\beta \cos\theta} \quad \text{(Eq. S1)}$$

where K was the shape factor (0.9), λ was the X-ray wavelength (1.5406 Å of Cu Kα source), β was the line broadening at FWHM after subtracting the instrumental line broadening, and θ was the Bragg angle.

All of the XPS spectra were deconvoluted by XPSPEAK41 after calibrating the major peak of C 1s to 284.8 eV. The binding energy of each peak in C 1s spectra was as follows: aromatic C at 284.8 eV, ketonic C and phenolic C at 286.0 eV, aliphatic C at 287.0 eV, and O-alkyl C at 289.1 eV. [1] As for the Cu species, the peaks of Cu(0)/Cu(I), CuO, and $Cu(OH)_2$ in Cu $2p_{3/2}$ spectra were at 932.6 eV, 933.7 eV, and 935.1 eV, respectively; while the peaks of Cu(0)/CuO and Cu_2O were at 568.2 eV and 570.0 eV, respectively. [2]

Regarding the MW absorbability, the energy distribution was directly determined by the analyzer, while the dielectric loss tangent (tan δ) was calculated by the Eq. S2, [3]

$$tan\,\delta = \frac{\varepsilon''}{\varepsilon'} \quad \text{(Eq. S2)}$$

where ε'' was the dielectric loss factor and ε'' was the relative dielectric constant. Both of them could be measured by the analyzer. It should be noted that the magnetic loss was not detected because there were no magnetic components in the Cu biochars.

The energy consumption (E) and average power (P, P_r or P_h) during the reaction were calculated following the Eqs. S3 and S4,

$$E = \int P_i dt \quad \text{(Eq. S3)}$$

$$P = \frac{E}{t} \quad \text{(Eq. S4)}$$

where P_i was the instant power recorded by the reactor and t was the time.

S3. Catalytic Performance

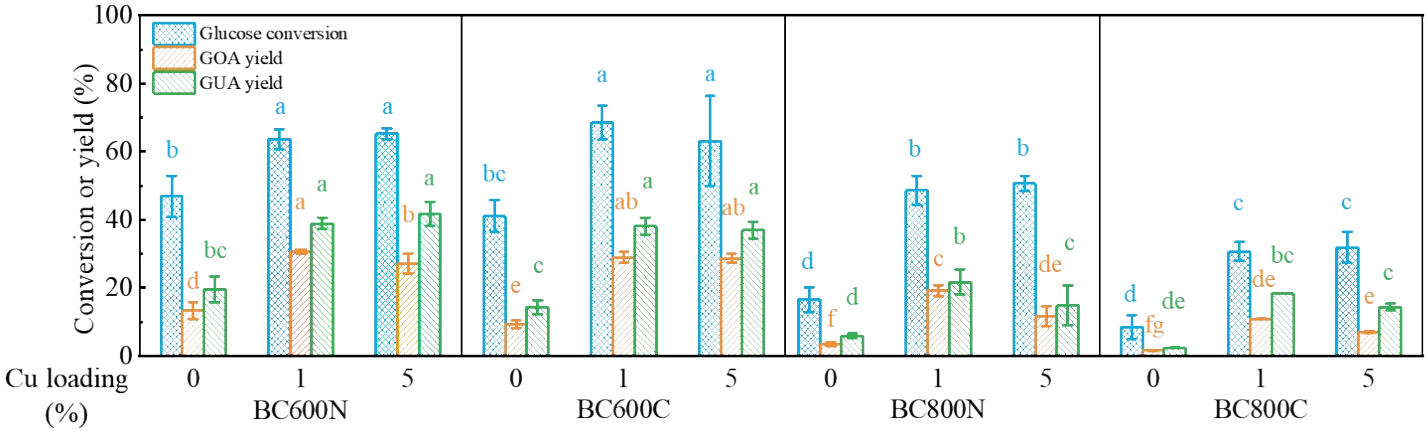

Fig. S1 Glucose conversion and yields of GOA and GUA over biochars with various Cu loading (reaction conditions: 200 mg glucose, 50 mg biochar, and 1 equiv. H_2O_2 in 10 mL DI water; 160 °C, 20 min). The lowercase letters indicate the significant levels of data.

***Control experiment** (reaction without catalyst): significance level of glucose conversion (24.2 ± 1.1%) is **cd**; while GOA or GUA were not detected.

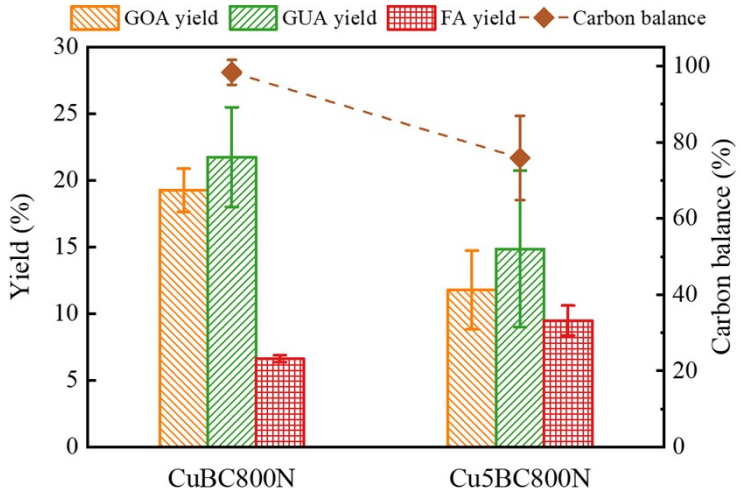

Fig. S2. Carbon balance and yields of GOA, GUA, and FA of glucose oxidation over CuBC800N and Cu5BC800N (reaction conditions: 200 mg glucose, 50 mg biochar, and 1 equiv. H_2O_2 in 10 mL DI water; 160 °C, 20 min)

The total selectivity of GOA and GUA is in the range of ca. 80 - 100% in most cases, while by-products including oxalic acid (yield < 1%), formic acid (yield < 10%), and fructose (yield

<1%) can be detected, ascribing to side reactions such as overoxidation and isomerization. The carbon balance is in the range of ca. 75 - 110%, where the lower values might be due to the generation of non-identifiable products or the mineralization of the organics, while the higher values could possibly be attributed to the high sensitivity of UV detector of HPLC, which could detect the small amount of dissolved organic matter of biochar, increase the intensity of known peaks, and plausibly increase the concentrations as a result.

The detectable organic acids with less C (*e.g.*, oxalic acid and formic acid) indicate the C-C cleavage and further evidence the over-oxidation. Besides, the decreased carbon balance also suggests the formation of non-identifiable products or mineralization to CO_2. For example, both GOA and GUA yields significantly decreased by ca. 7% with the Cu loading on BC800N increasing from 1% to 5%, because of the over-oxidation supported by the decrease of carbon balance and the increased formic acid yield (**Fig. S2**).

S4. Supplementary Results of Cu Biochar Characterization

S4.1 Overall characteristics

Table S1 Physicochemical properties of Cu biochar catalysts

Catalyst		CuBC600N	CuBC600C	CuBC800N	CuBC800C
Elemental Analysis	C/wt%	87.89	86.79	88.12	88.04
	H/wt%	1.25	1.24	0.75	0.62
	N/wt%	0.15	0.14	0.00	0.06
	O/wt% [a]	6.36	8.13	6.78	7.23
	Ash/wt%	4.35	3.70	4.35	4.05
	H/C [b]	0.171	0.171	0.102	0.085
	O/C [b]	0.054	0.070	0.058	0.062
pH before reaction [c]		5.93	6.04	6.45	6.32
Pore structure	BET surface area/m^2 g^{-1}	110.4	254.1	323.8	358.1
	BJH average pore diameter/nm	4.66	3.85	4.36	5.29
Glucose adsorption/% [d]		2.41	3.05	4.30	3.60

a, calculated by equation: m(O) = m(total) – m(C) – m(H) – m(N) – m(ash); b, atom ratio; c, 0.1 g glucose and 25 mg biochar in 5 mL DI water, rotated at 30 rpm for 4 h; d, 0.1 g glucose and 25 mg biochar in 5 mL DI water, rotated at 30 rpm for 12 h

Regarding the impurities of biochar, the total ash contents of the biochar without Cu are in the range of 2.2~2.9 wt.%. According to ICP-OES results, Si was the primary element (~1.6 wt.%), Ca was the secondary element (~0.4 wt.%), and other elements (*e.g.*, K, Na, Al, and Fe) with much lower contents were also detected. Therefore, the dominant impurity in biochar

should be silicate, which is catalytically inactive, while Ca might play roles for glucose isomerization towards fructose, [2] and the fructose yield of <1% was detected.

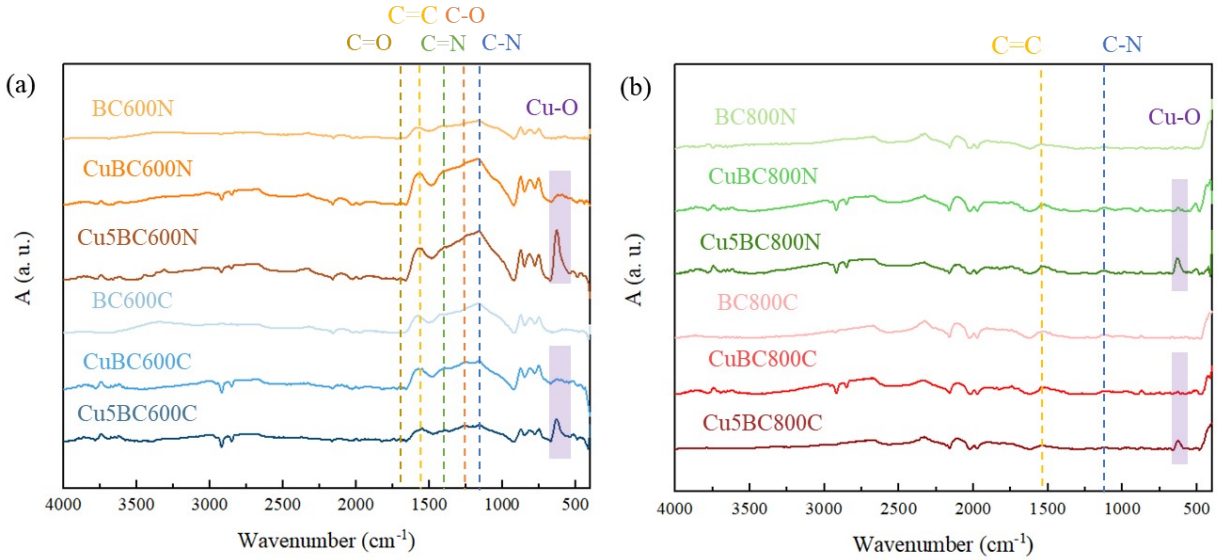

Fig. S3 FTIR spectra of biochar samples pyrolysis at (a) 600 °C and (b) 800 °C

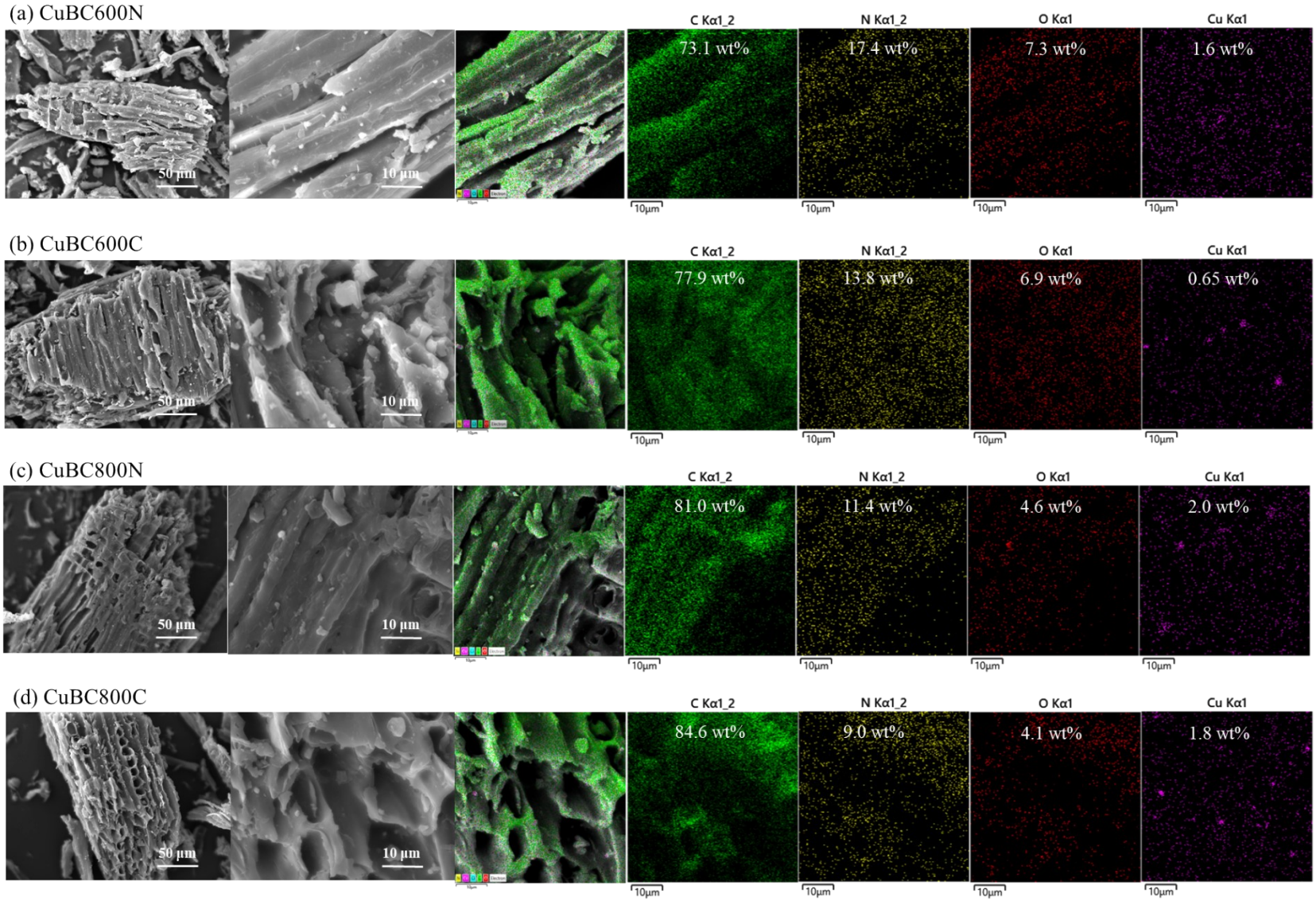
(a) CuBC600N
50 µm
10 µm
C Kα1_2
73.1 wt%
N Kα1_2
17.4 wt%
O Kα1
7.3 wt%
Cu Kα1
1.6 wt%
10µm
(b) CuBC600C
50 µm
10 µm
C Kα1_2
77.9 wt%
N Kα1_2
13.8 wt%
O Kα1
6.9 wt%
Cu Kα1
0.65 wt%
10µm
(c) CuBC800N
50 µm
10 µm
C Kα1_2
81.0 wt%
N Kα1_2
11.4 wt%
O Kα1
4.6 wt%
Cu Kα1
2.0 wt%
10µm
(d) CuBC800C
50 µm
10 µm
C Kα1_2
84.6 wt%
N Kα1_2
9.0 wt%
O Kα1
4.1 wt%
Cu Kα1
1.8 wt%
10µm

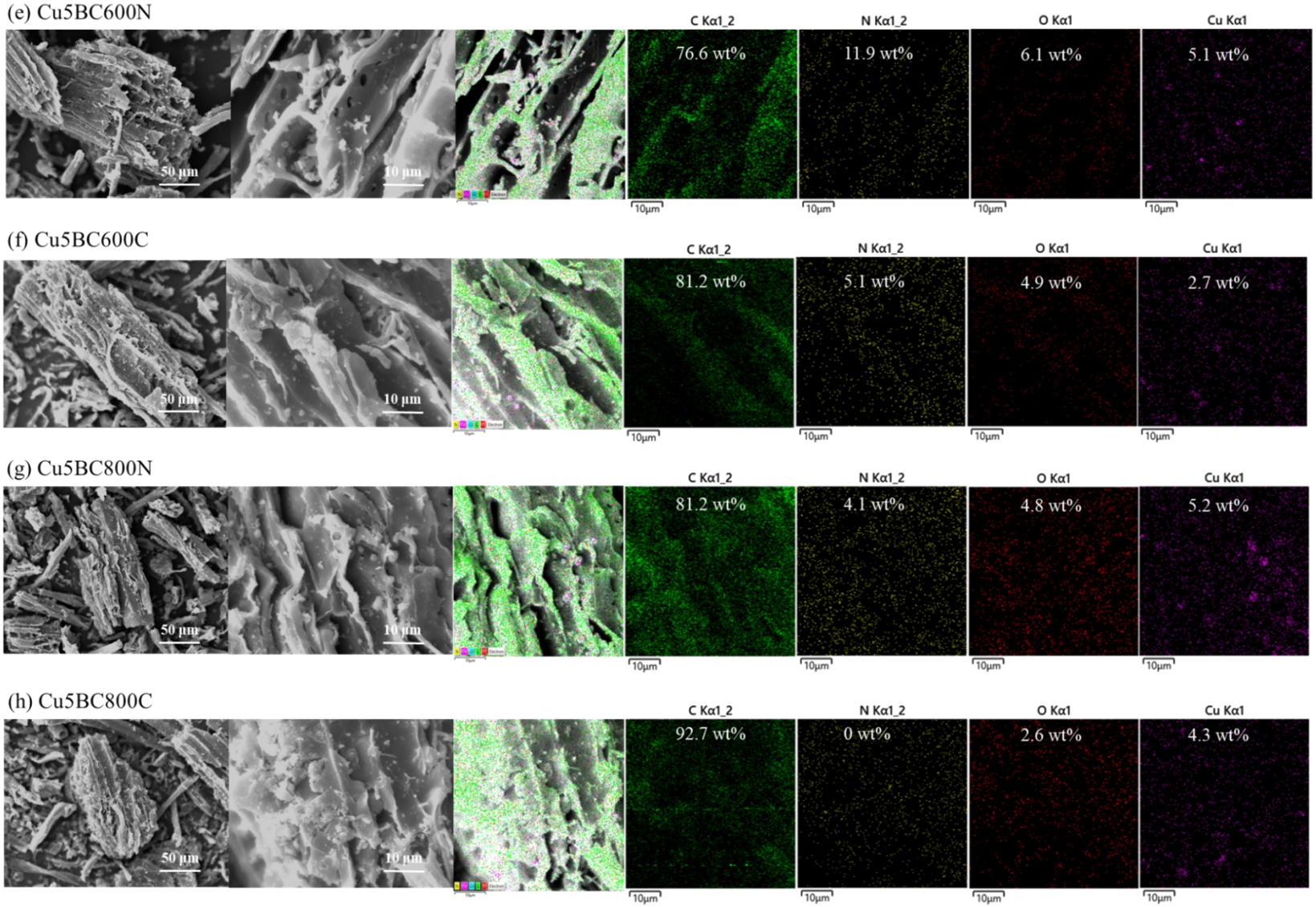

Fig. S4 SEM-EDX images of Cu biochar catalysts.

S4.2 Loaded Cu Particles

Table S2 Cu loading and major crystal phases in biochar catalysts

Cu biochar	Pyrolysis T/°C	Purging gas	Cu loading/wt%	Mean size of Cu_2O*/nm	Mean size of Cu*/nm	$I_{111}(Cu_2O)/I_{111}(Cu)^{\#}$
CuBC600N	600	N_2	1.1±0.1	21.9	29.7	1.75
CuBC600C	600	CO_2	1.1±0.0	22.1	38.7	1.02
CuBC800N	800	N_2	1.1±0.0	27.7	39.9	0.56
CuBC800C	800	CO_2	0.9±0.2	22.1	34.4	1.29
Cu5BC600N	600	N_2	5.5±0.0	22.4	40.5	0.90
Cu5BC600C	600	CO_2	5.2±0.4	21.7	39.5	0.84
Cu5BC800N	800	N_2	5.7±0.4	20.7	39.4	0.41
Cu5BC800C	800	CO_2	5.3±0.5	19.2	41.1	0.38

* Mean sizes of major crystal phases were calculated by Scherrer equation based on XRD patterns; # The intensity ratio of $Cu_2O(111)$ and $Cu(111)$ (2θ = 36.2 and 43.1°, respectively)

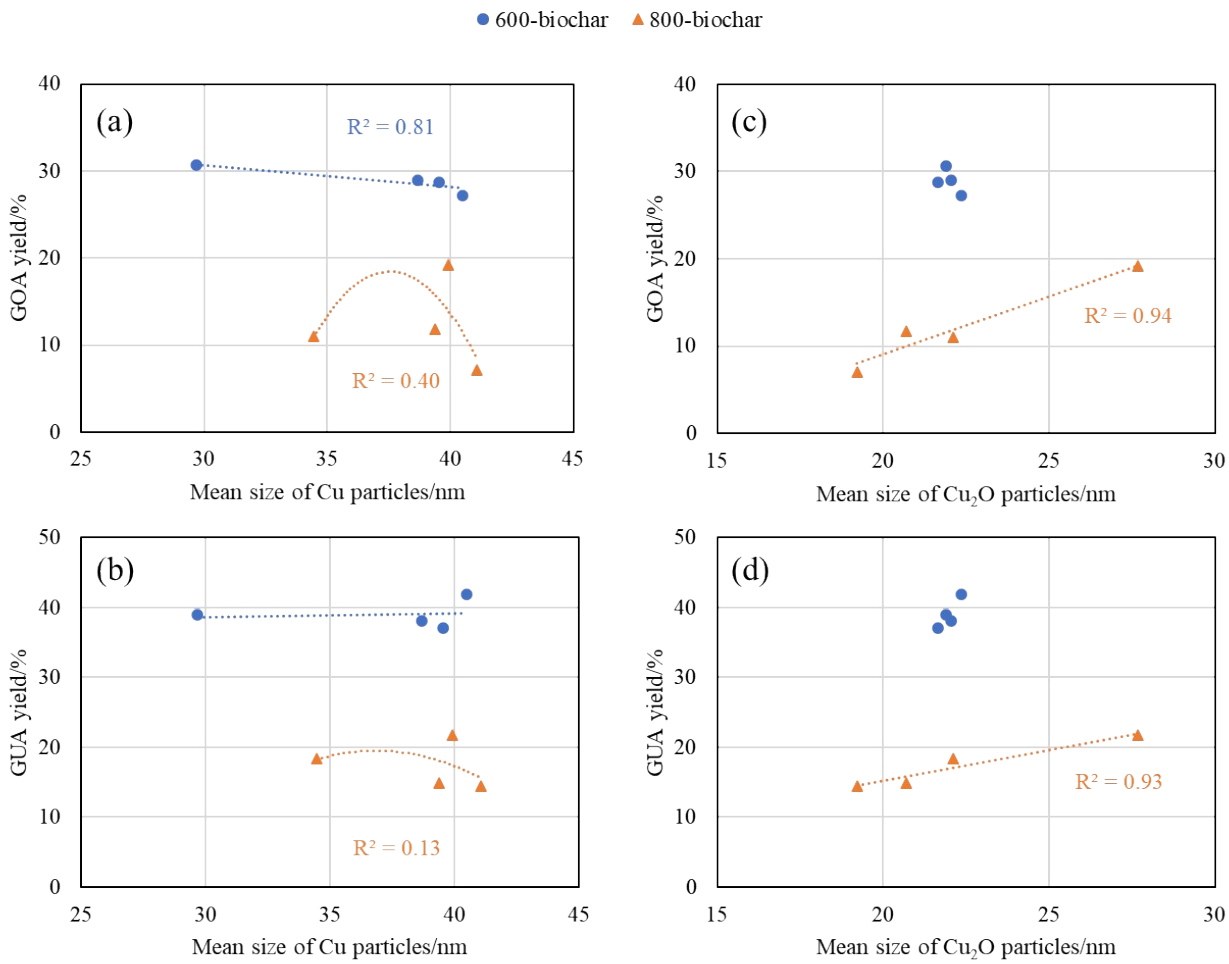

Fig. S5 Relationships between sizes of Cu_2O/Cu and yields of GOA/GUA (Reaction conditions: 200 mg glucose, 50 mg biochar, and 1 equiv. H_2O_2 in 10 mL DI water; 160 °C)

The crystal phases Cu, Cu_2O, and CuO were corresponding to PDF #04-0836, PDF #05-0667, and PDF #44-0706, respectively. The sizes of crystal phases were calculated based on Scherrer equation (**Table S2**). To investigate the property-performance relationships, we correlated the size of crystal particles (*i.e.*, Cu_2O and Cu) and the catalytic performances (*i.e.*, the GOA and GUA yield) based on groups by synthesis temperature (**Fig. S5**) to exclude the significant effects of support on catalytic performances (**Fig. S10**). As shown in **Fig. S5a** and **S5b**, the catalytic performances for 600°C biochar catalysts were not significantly influenced by the size of Cu, while a possible volcano relationship between catalytic performance and Cu size can be found for 800°C biochar catalysts. Yet, this relationship may not be convincing, due to the limited data (only 4 points), the narrow range of the particle size (~ 6 nm), and the relatively low values of R^2. Similarly, the very narrow size range (~ 1.5 nm) of the Cu_2O in 600°C biochar was also observed (**Fig. S5c** and **S5d**). Whereas, for 800°C biochar catalysts, a positive correlation between catalytic performance and Cu_2O size can be observed in the range from ~ 19 to ~ 27 nm, providing information for future research regarding the particle size effects.

S4.3 Biochar supports

The wavenumber of each band in Raman spectra was as follows: S band at 1257 cm^{-1}, D band at 1352 cm^{-1}, Ar_1/Ar_2 band at 1437/1515 cm^{-1}, and $G^{-/+}$ band at 1588/1602 cm^{-1}. [4] As shown in the spectra (**Fig. S7b**), the amorphous area including S, D and Ar_1 bands significantly narrowed when pyrolysis temperature increased from 600°C to 800°C, indicating the formation of more ordered biochar. Specifically, the percentage of S band (sp^3-rich structures) did not show a considerable difference in this temperature range. According to the further analyzed data, it was noted that the intensity ratio of D band to Ar band (I_D/I_{Ar}) significantly improved from ca. 0.4 to ca. 0.9 ~ 1.3, as a result of the simultaneous increase of D band (aromatic system with ≥ 6 rings) and decrease of Ar band (aromatic system with 3 ~ 5 rings). This change suggested the condensation of aromatic rings with temperature increasing, in accordance with the dehydrogenation supported by the decreased H/C ratio, which could also lead to the significantly increased light absorbing ability, evidenced by the decrease of total intensity of spectra. [5] On the other hand, it was noted that the G^- band was blue-shifted to G^+ when pyrolysis temperature increased, especially under N_2 purging, which could be probably attributed to the single-double carbon bond alternation and the formation of defects. [7]

As presented in the TG-DTG-DSC Profiles under N_2 or CO_2 atmosphere (**Fig. S6**), the trends of TG and DTG curves were of considerable similarity. The pyrolysis temperature of

cellulose and hemicellulose (200 ~ 400°C) could be respectively decreased by ca. 10 and 40°C with 1% and 5% Cu loading, indicating the catalytic effect of Cu during the pyrolysis. [8] The corresponding upward peaks in DSC curves evidenced the endothermic decomposition of the polysaccharides. Then, it could be speculated that the carbon matrix formed at ca. 400°C because the mass of all the studied samples changed slightly when the temperature was further increased (> 400°C). Therefore, the DSC profiles could directly present the thermal effect of each sample in this temperature range. Under N_2 environment (**Fig. S6a**), the DSC profiles of raw biomass and 5% Cu-loaded biomass both presented a broad peak of exothermal carbonization in the range of 500 ~ 750°C, resulting in more pore structure [6, 9]; while this peak was shifted to 400 ~ 650°C in the profile of 1% Cu-loaded biomass, indicating the different catalytic effect due to the low loading Cu. As for the overall trend with temperature increasing, more Cu loading resulted in an earlier uptrend corresponding to the beginning stage of endothermic graphitization. [6] As for the pyrolysis with CO_2 purging (**Fig. S6b**), the area of carbonization peaks in the profiles of raw biomass and 1% Cu-loaded biomass were significantly larger than those under the N_2 atmosphere, which might be the reason for higher porosity (*e.g.*, higher specific surface area and pore diameter) of samples prepared at 800°C with CO_2 purging.

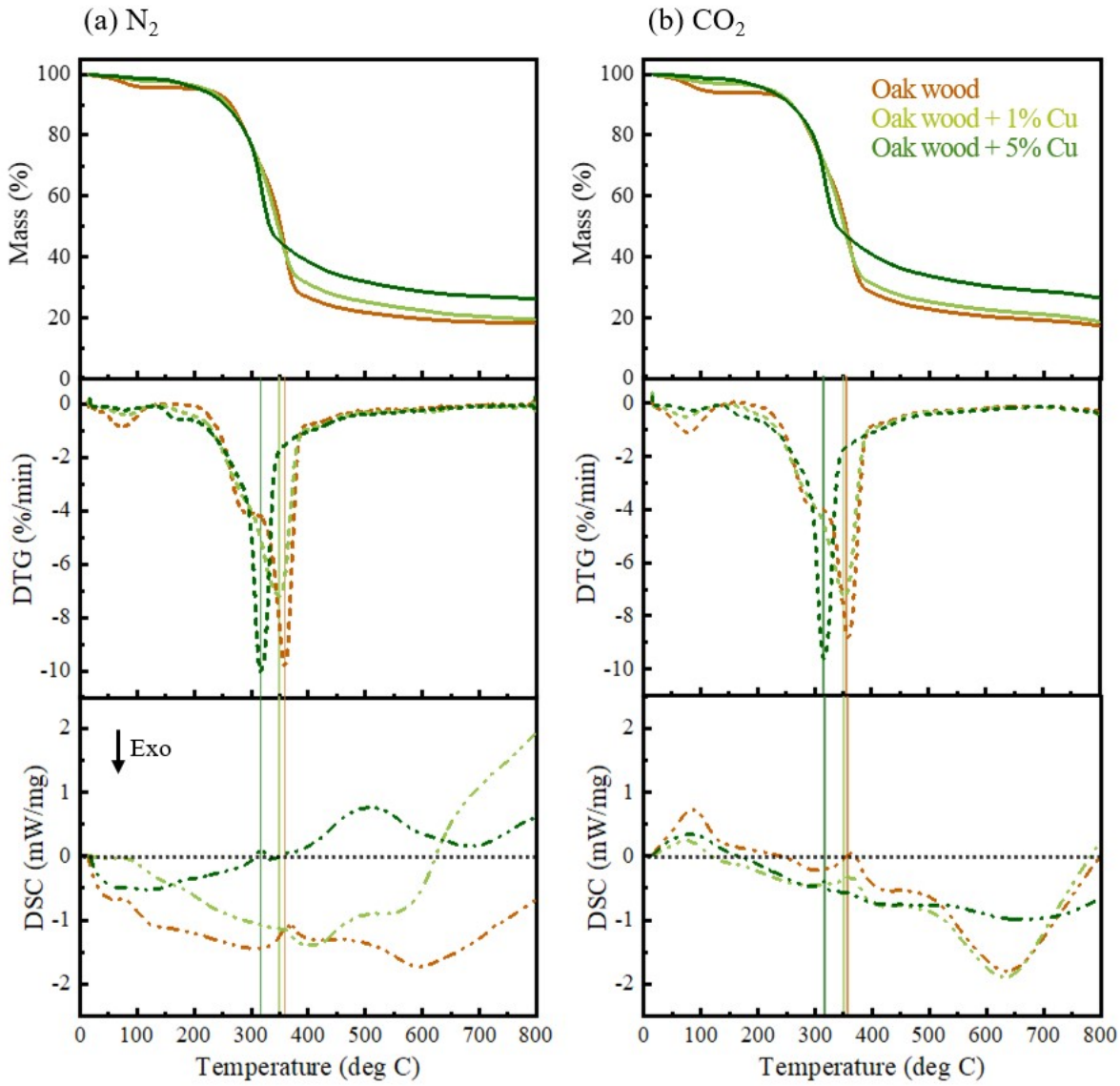

Fig. S6 TG-DTG-DSC curves of biomass materials under N_2 (a) and CO_2 (b) atmosphere.

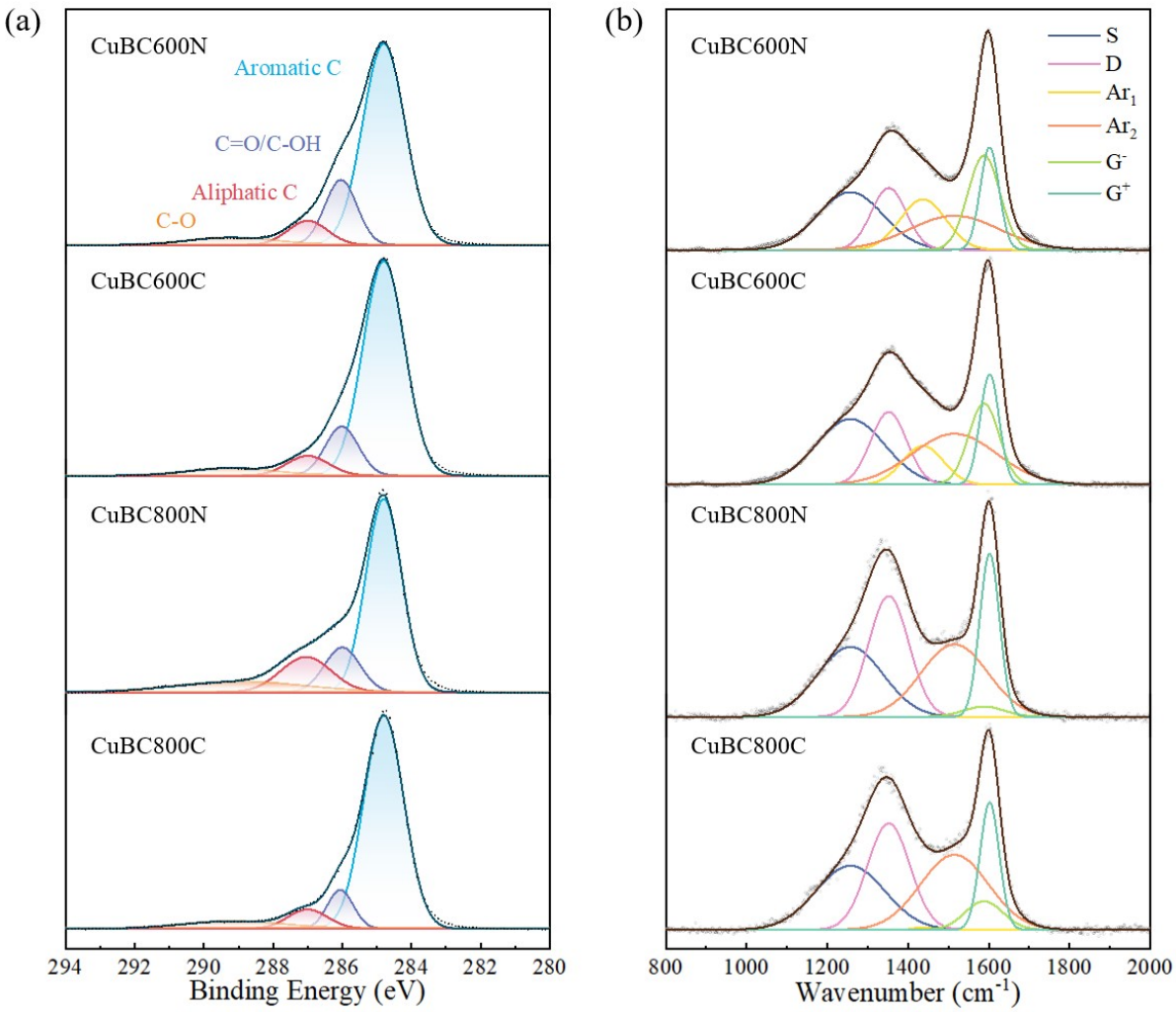

Fig. S7 XPS C 1s (a) and Raman (b) spectra of Cu biochar catalysts with deconvoluted peaks

Table S3 Summary of C 1s XPS and Raman spectra deconvolution results of Cu biochar catalysts.

Catalyst		CuBC600N	Cu5BC600N	CuBC600C	Cu5BC600C	CuBC800N	Cu5BC800N	CuBC800C	Cu5BC800C
Intensity in XPS spectra/%	Aromatic C	69.9	80.0	74.4	79.9	59.7	71.1	77.5	75.5
	Ketonic C, C=O; phenolic C, C-OH	17.2	10.2	13.5	9.0	13.8	13.9	9.1	8.6
	Aliphatic C, CH_3, CH_2, CH	7.9	4.6	6.9	6.5	15.4	8.9	6.9	5.0
	O-alkyl C, C-O	5.1	5.2	5.1	4.6	11.2	6.1	6.5	10.8
Intensity in Raman spectra/%	S	23.3	25.2	25.6	25.1	25.5	25.1	25.0	25.2
	D	13.4	15.8	14.8	13.1	27.2	29.2	25.7	26.8
	Ar	32.9	34.2	33.5	35.5	27.0	23.2	29.3	27.3
	G^-	18.6	11.1	14.1	13.5	2.4	6.3	6.1	5.1
	G^+	11.9	13.7	11.9	12.7	17.9	16.2	13.9	15.7
Total Intensity ($\times 10^5$)		15.7	12.6	13.7	14.3	3.1	3.4	3.0	2.6
I_D/I_G		0.44	0.64	0.57	0.50	1.34	1.30	1.28	1.29
I_D/I_{AR}		0.41	0.46	0.44	0.37	1.01	1.26	0.88	0.98

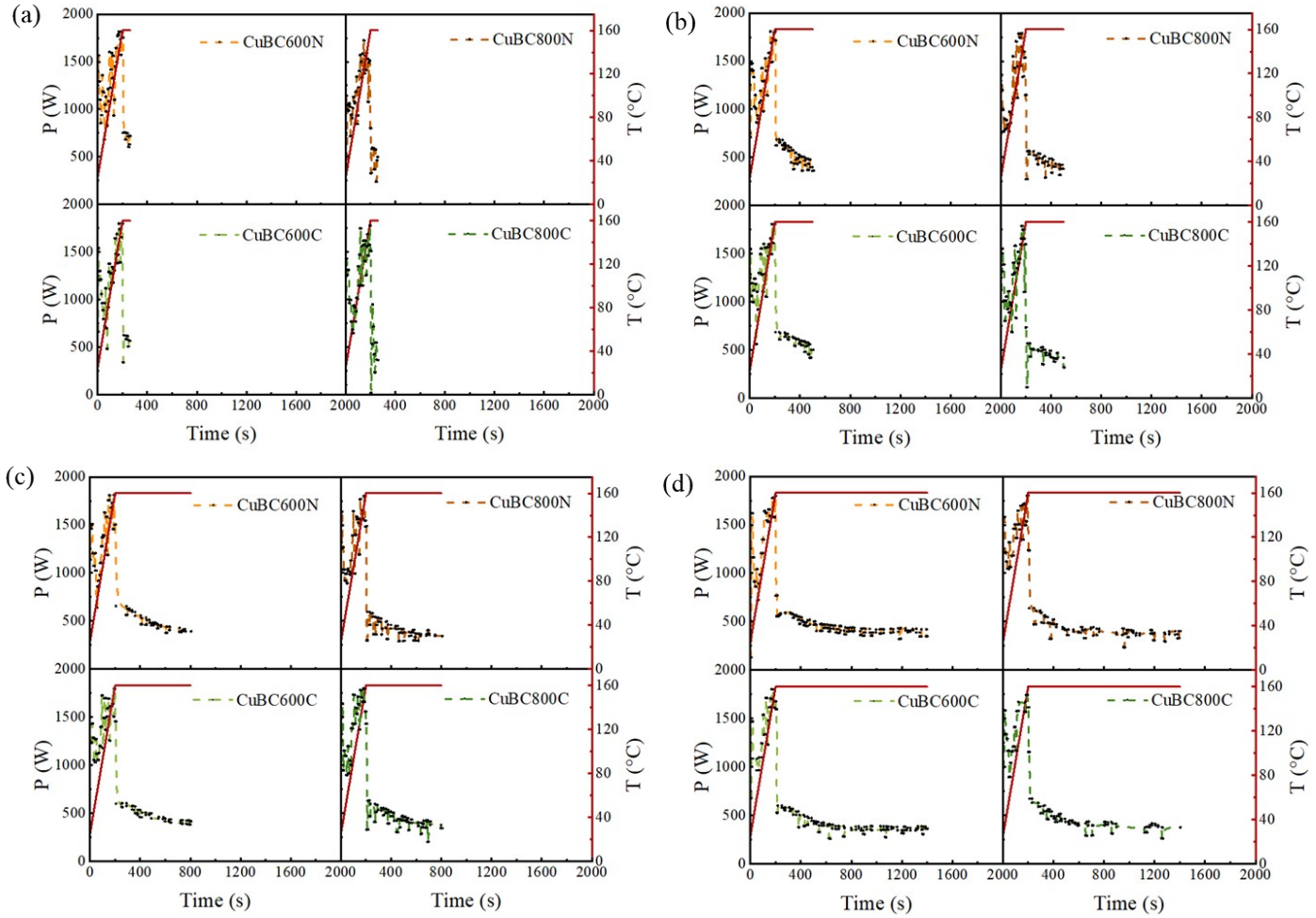

S5. Microwave Energy Consumption Profiles

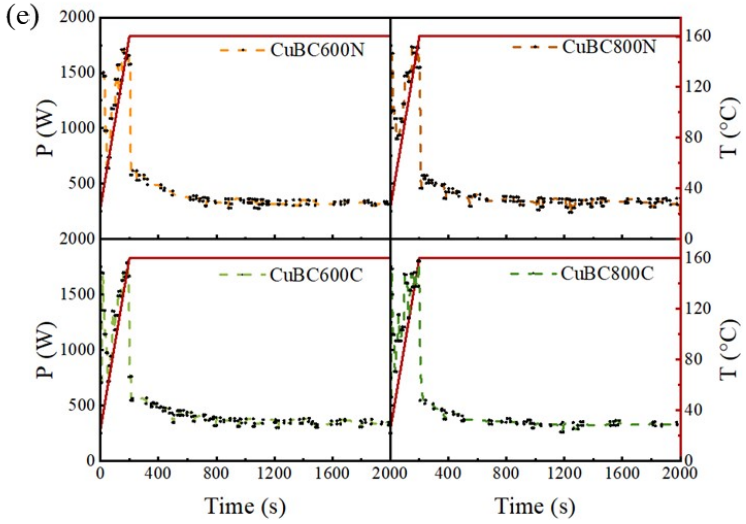

Fig. S8 Power and temperature profiles during reaction for different time (a) 1 min, (b) 5 min, (c) 10 min, (d) 20 min, and (e) 30 min.

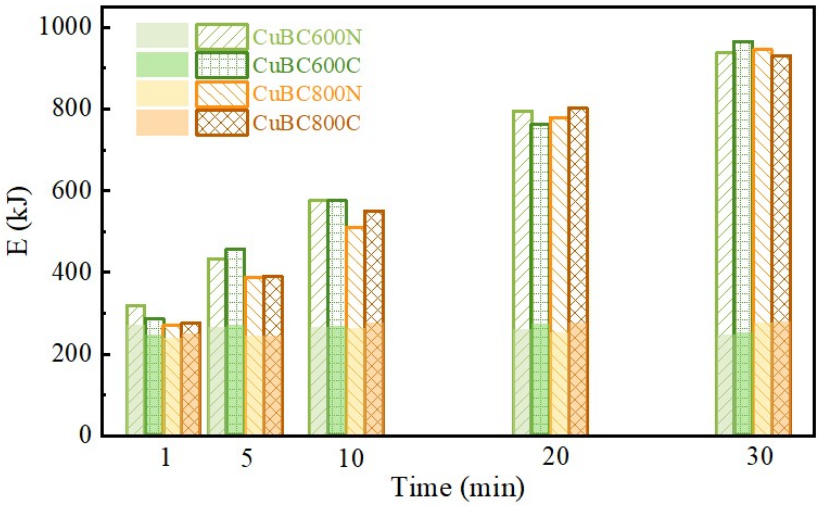

Fig. S9 Energy consumption during reaction (pattern-filled column: total energy consumption; colour-filled part: energy consumption during the ramping stage; reaction conditions: 200 mg glucose, 50 mg biochar, and 1 equiv. H_2O_2 in 10 mL DI water; 160 °C)

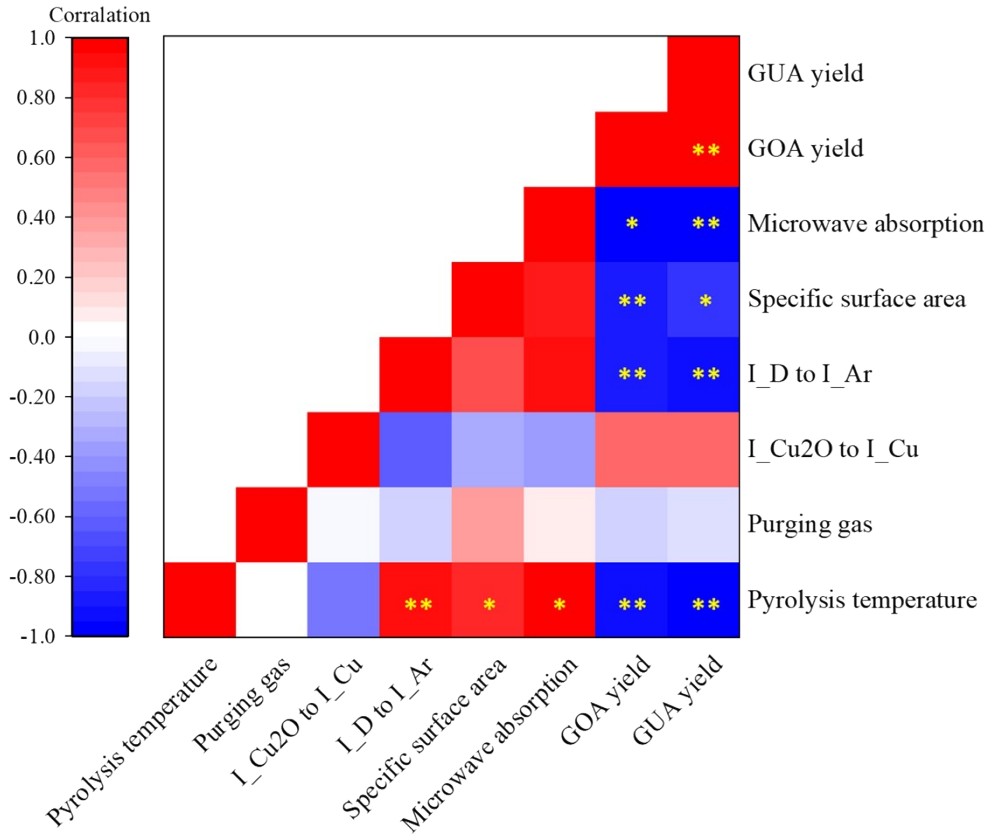

Fig. S10 Correlation matrix of synthesis conditions, characteristics, and catalytic performances of Cu biochar catalysts (**p < 0.01, *p < 0.05)

S6. Recyclability and stability

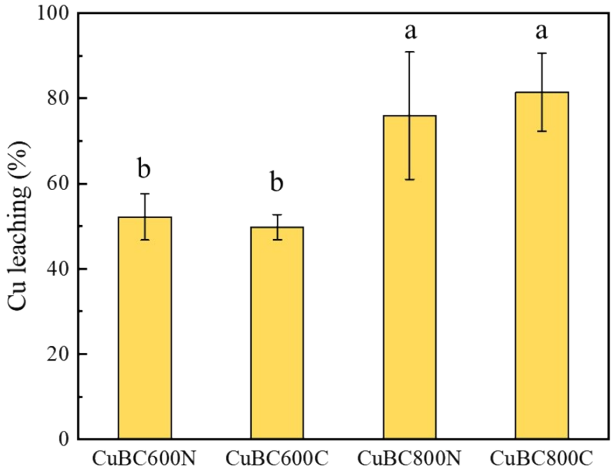

Fig. S11 Cu leaching rate of Cu biochar catalysts after reaction (reaction conditions: 200 mg glucose, 50 mg biochar, and 1 equiv. H_2O_2 in 10 mL DI water; 160 °C, 20 min). The lowercase letters indicate the significant levels of data.

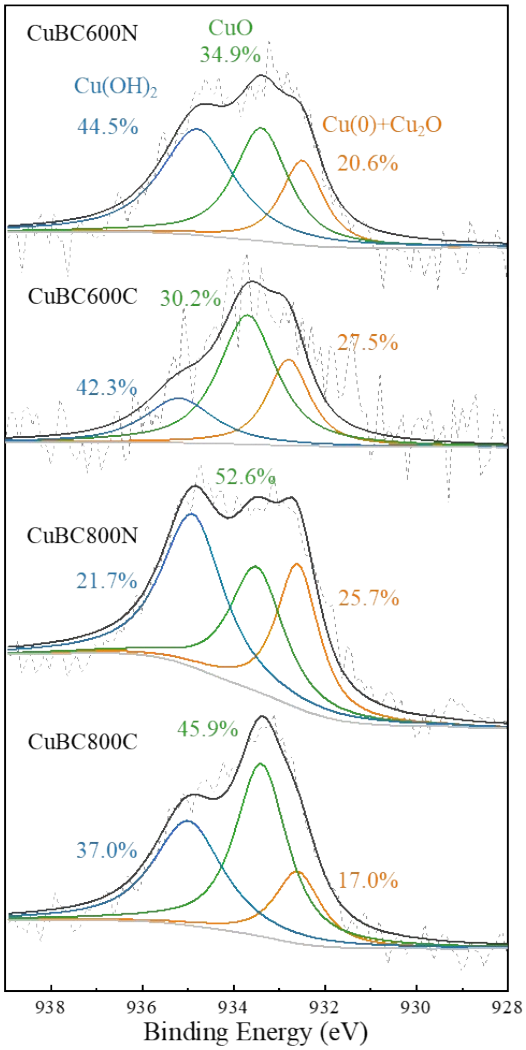

Fig. S12 XPS Cu 2p spectra of spent Cu-biochar catalysts

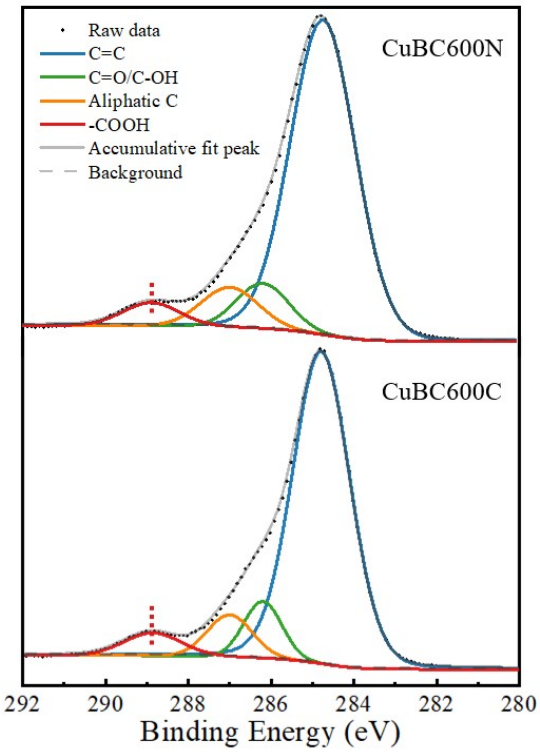

Fig. S13 XPS C 1s spectra of CuBC600N and CuBC600C after three-run reaction

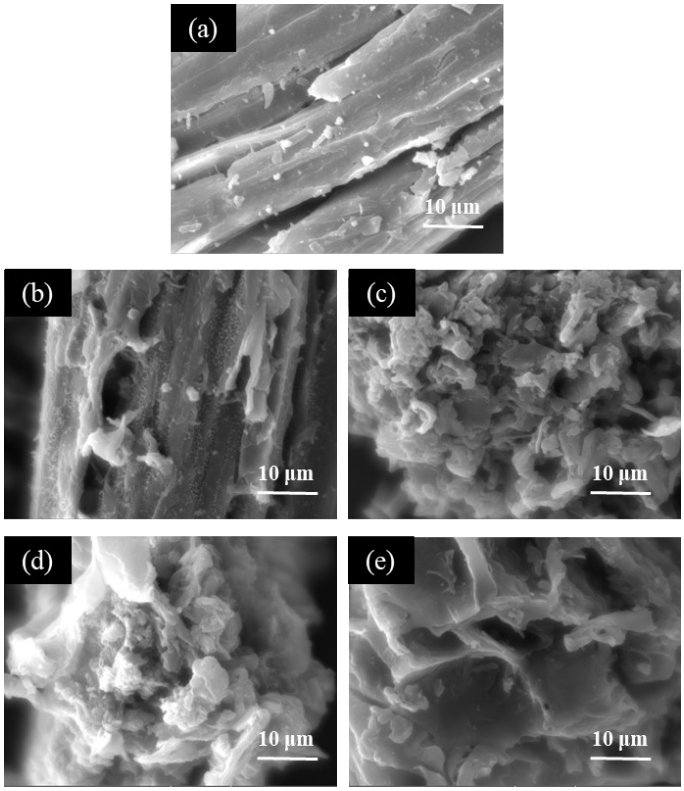

Fig. S14 SEM images (5000×) of (a) CuBC600N, (b) CuBC600N-r1, (c) CuBC600N-r3, (d) CuBC600N-r1*, and (e) CuBC600N-r1** (reaction conditions: 200 mg glucose, 50 mg biochar, and 1 equiv. H_2O_2 in 10 mL DI water; 160 °C, 20 min; r1*: no glucose, r1**: no glucose and H_2O_2)

According to the XPS Cu 2p spectra (**Fig. 3** and **Fig. S12**), it is found that the proportion of Cu_2O/Cu significantly decreased after reaction while those of the Cu(II) species (*i.e.*, CuO and $Cu(OH)_2$) increased accordingly. Based on the analysis of mechanisms, the Cu/Cu_2O are the active sites for reaction. The converted surface species is a plausible reason of the deactivation apart from the Cu leaching. Whereas, as shown in the XPS C 1s spectra of the catalysts after 3 runs (**Fig. S13**), the peak of -COOH at 288.8 eV was detected with considerable intensity, which was not detected in the pristine catalysts. The appearance of this peak implies the adsorption of oxidative products containing -COOH. The SEM images (**Fig. S14**) show that the surface of biochar was destructed after reactions. The resulting improvement of pore structure might play the positive roles as it has been found that the pore structure favours the microwave interactions. By comparing **Fig. S14 (a)**, **(b)**, **(d)**, and **(e)**, the destruction of biochar might be mainly attributed to the microwave-assisted hydrothermal effect and existence of H_2O_2.

According to the reaction by using filtrate (**Fig. S15**), it is found that the carbon balance is significantly lower than that over biochar due to the production of unknown by-products. These findings indicate the lower selectivity and atomic efficiency, which can also be supported by the slightly higher yield of over-oxidation by-product formic acid. Furthermore, the role of biochar support for selectivity can be evidenced.

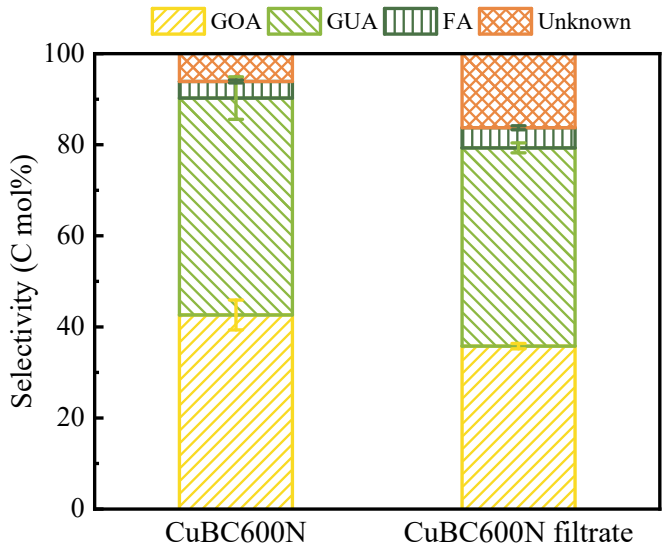

Fig. S15. Product selectivity of glucose oxidation catalyzed by CuBC600N and its filtrate (Conditions before filtration: 50 mg biochar and 10 mL DI water, 160 °C, 10 min; Reaction conditions: 200 mg glucose and 1 equiv. H_2O_2 in 10 mL leachate, 160 °C, 10 min)

S7. DFT simulation

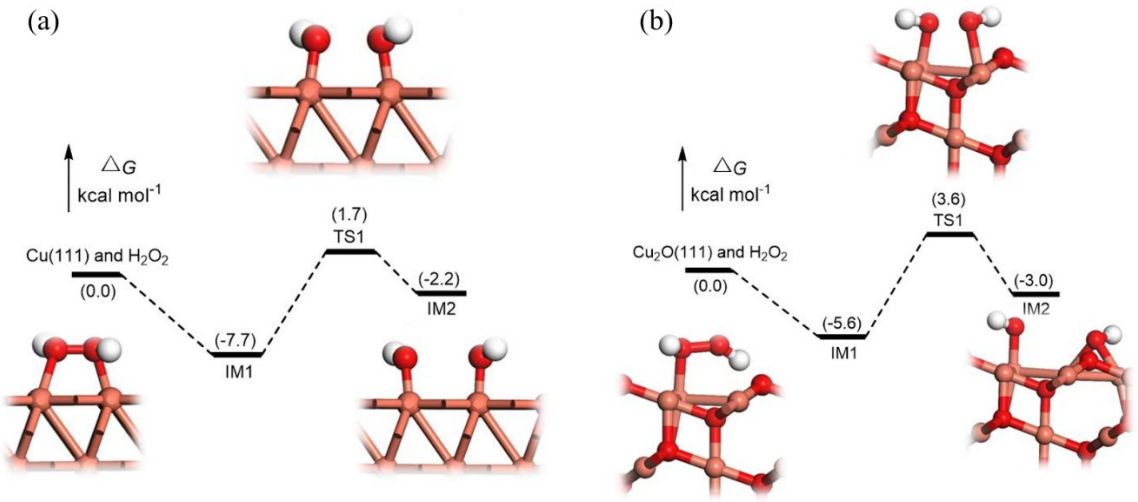

Fig. S16 Energy profiles of H_2O_2 dissociation over (a) Cu(111) and (b) Cu_2O(111)

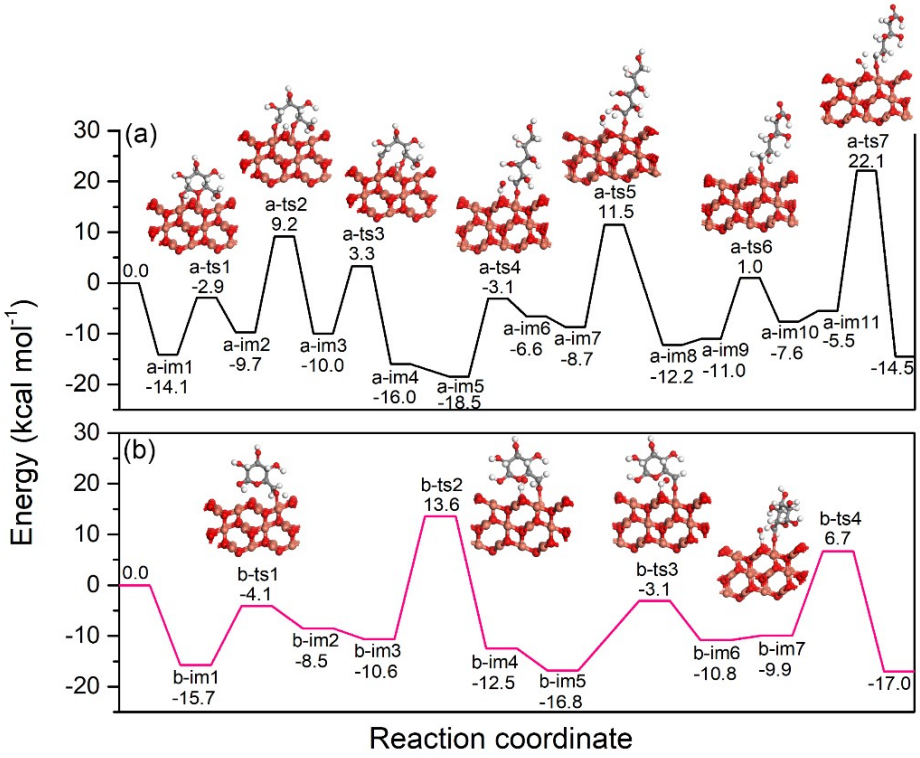

Fig. S17 Energy profiles of cyclic glucose conversion to GUA over Cu_2O(111) (a) via ring-opening step, and (b) direct conversion

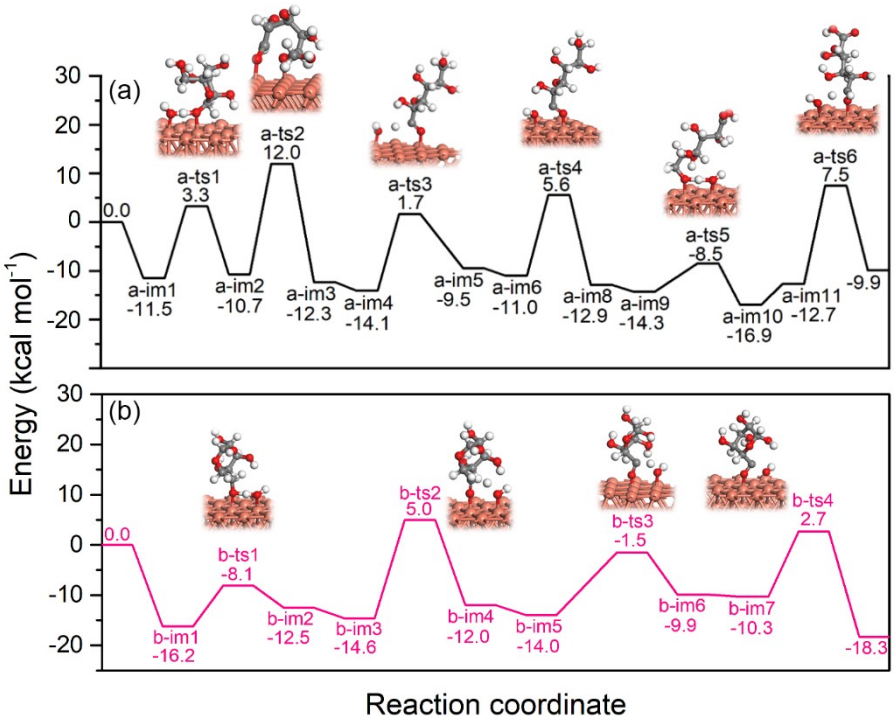

Fig. S18 Energy profiles of cyclic glucose conversion to GUA over Cu(111) (a) via ring-opening step, and (b) direct conversion

The adsorption energies onto Cu(111) and $Cu_2O(111)$ surface were determined as -16.8 and -14.1 kcal mol^{-1}, respectively, indicating that the adsorption process are both thermodynamically spontaneous.

The specific pathways over Cu_2O (**Fig. S17**) are discussed as follows. After the adsorption of glucose onto $Cu_2O(111)$, hydroxyl H in -C(1)H_2-OH migrated to O of $Cu_2O(111)$ with a 11.2 kcal mol^{-1} energy barrier, which induced the breaking of C1-O, giving an 18.9 kcal mol^{-1} energy barrier. The ring-opening was completed to obtain chain glucose by the H in $Cu_2O(111)$ returning to C5-O, the energy barrier of which was 13.3 kcal mol^{-1}. Then, ·OH derived from the dissociation of H_2O_2 could attack C in -HC(6)=O of cyclic glucose, and H in -HC(6)=O subsequently migrated to another ·OH to form water, thus obtaining GOA. The energy barriers of the two processes were 15.4 and 20.2 kcal mol^{-1}, respectively. As for the formation of GUA, two possible reaction pathways (**Scheme 1**) were taken into considerations: the oxidation of GOA to GUA by –C(6)H_2-OH to –HC=O and the oxidation of cyclic glucose to GUA by –C(6)H_2-OH to –COOH. It was calculated in the former pathway that hydroxyl H in –C(6)H_2-OH could shift onto $Cu_2O(111)$ to form –C(6)H_2-O, and H in –C(6)H_2-O was subsequently removed by ·OH, giving the formation of GUA (**Fig. S17a**), the energy barriers of which were 12.0 and 27.6 kcal mol^{-1} (*i.e.*, rate-controlling step with the highest energy barrier),

respectively. As a comparison, the reaction pathways over Cu(0) was also investigated to clarify the synergistic effects of Cu(0)/Cu(I) species on the conversion of glucose to GOA and GUA. The specific pathways are similar to those over $Cu_2O(111)$ as shown in **Fig. S18**. The quantitative comparison can be seen in **Section 3.6** in the main text.

References

1. B. Singh, Y. Fang, B. C. C. Cowie and L. Thomsen, *Organic Geochemistry*, 2014, **77**, 1-10.
2. R. B. Ilia Platzman, Hossam Haick, Rina Tannenbaum, *J Phys Chem C*, 2008, **112**, 1101-1108.
3. R. Wei, P. Wang, G. Zhang, N. Wang and T. Zheng, *Chemical Engineering Journal*, 2020, **382**, 122781.
4. S. S. Chen, Y. Cao, D. C. W. Tsang, J.-P. Tessonnier, J. Shang, D. Hou, Z. Shen, S. Zhang, Y. S. Ok and K. C. W. Wu, *ACS Sustainable Chemistry & Engineering*, 2020, **8**, 6990-7001.
5. X. Li, J. Hayashi and C. Li, *Fuel*, 2006, **85**, 1700-1707.
6. S. Yoo, C.-C. Chung, S. S. Kelley and S. Park, *ACS Sustainable Chemistry & Engineering*, 2018, **6**, 9113-9119.
7. K. N. Kudin, B. Ozbas, H. C. Schniepp, R. K. Prud'homme, I. A. Aksay and R. Car, *Nano Letters*, 2008, **8**, 36-41.
8. M. M. Emara, S. H. Ali, T. S. E. Kassem and P. G. Van Patten, *Journal of Nanoparticle Research*, 2020, **22**.
9. Z. Li, W. Lv, C. Zhang, B. Li, F. Kang and Q. Yang, *Carbon*, 2015, **92**, 11-14.